Applied Catalysis B: Environmental 243 (2019) 415–427

Contents lists available at ScienceDirect

Applied Catalysis B: Environmental

journal homepage: www.elsevier.com/locate/apcatb

# Synthesis and characterization of AMO LDH-derived mixed oxides with various Mg/Al ratios as acid–basic catalysts for esterification of benzoic acid with 2-ethylhexanol

J. Kuljiraseth[a,d], A. Wangriya[b], J. M.C. Malones[a], W. Klysubun[c], S. Jitkarnka[a,d,*]

[a] The Petroleum and Petrochemical College, Chulalongkorn University, Phayathai Rd. 254, 10330, Bangkok, Thailand
[b] SCG Chemicals Co Ltd, 1 Siam Cement Rd, Bangsue, Bangkok, 10800, Thailand
[c] Synchrotron Light Research Institute, Muang District, 111 University Avenue, Nakhon Ratchasima, 30000, Thailand
[d] Center of Excellence on Petrochemical and Materials Technology, Bangkok, Thailand

ARTICLE INFO

*Keywords:*
XAS
LCF
Mg K-edge
Al K-edge
Esterification
Benzoic acid
AMO-LDHs

ABSTRACT

Proven to possess distinguishable physical and acid-base properties superior to conventional LDHs, Aqueous Miscible Organic solvent-Layered Double Hydroxides (AMO-LDHs) were thus synthesized and used as precursors to prepare the Mg/Al mixed oxide catalysts in this work. The AMO-LDH based oxide catalysts with various ratios of Mg/Al were studied for the chemical and physical properties and the activity on esterification of benzoic acid with 2-ethylhexanol. The catalysts were characterized using BET, XRD, TGA, and XPS. Moreover, the acid-base properties were studied by using $NH_3$-TPD, $CO_2$-TPD, and X-ray Absorption Spectroscopy (XAS) techniques, both XANES and EXAFS. As a result, the Mg/Al mixed oxides after calcination at 500 °C still had the clay structure, and were found to possess both acid and base sites. As the Mg/Al ratio increased, the total density of acid and basic sites decreased. Moreover, the acid-basic strength depended on their phase compositions and coordination number. The activity of calcined LDHs catalysts was tested for the esterification of benzoic acid with 2-ethylhexanol, aimed at producing 2-ethylhexyl benzoate as the desired chemical. The products were analyzed using GC–MS/TOF. In summary, the conversion of benzoic acid was enhanced significantly using the Mg−Al mixed oxides as the catalysts, owing to the acid-base sites (both $Mg^{2+}-O^{2-}$ and $Al^{3+}-O^{2-}$ pairs) of the catalysts. The catalyst with the Mg/Al ratio of 4:1 can convert 66% benzoic acid to 2-ethylhexyl benzoate. Moreover, the other products were composed of 2-ethylhexanal, 3-heptanone, and 3-heptanol because of acid-base pairs.

## 1. Introduction

Benzoic acid, a major component in many acid wastes from various production plants, can be used to produce valuable chemicals such as 2-ethylhexyl benzoate via esterification reaction with 2-ethyhexanol [1]. Normally, homogeneous catalysts were commonly used in this reaction, such as inorganic acid [2], Lewis acid [3], and metallic compounds [4]; however, they several disadvantages such as toxicity, corrosiveness, and difficulty to separate from the reaction medium. As substitutes for homogeneous catalysts to overcome the disadvantages, several kinds of heterogeneous catalysts, such as Amberlyst [5], $SnO/Al_2O_3$, [6], $ZnAl_2O_4$ [7], and $ZrO_2/SiO_2$ [8], have been studied and found to the enhance the esterification reaction. As illustrated in Scheme 1, based on various references, the esterification of benzoic acid with 2-ethyhexanol produces 2-ethylhexanol benzoate on acid-base sites [1,9]. However, 2-ethylhexanol can be converted to other products. For instances, the oxidation of 2-ethylhexanol to 2-ethylhexanal [10] can take place on an acid-based site [11] of a catalyst with a low content of Al [12]. Then, 2-ethylhexanoic acid can be formed from 2-ethylhexanal [10] on an acid site [13]. Subsequently, 2-ethylhexanoic acid can be converted to 3-heptanone [14] via ketonization by a basic site [15]. Furthermore, 3-hepatnol can be formed from the hydrogenation of 3-heptanone [16] over acid-basic sites [17,18]. It can be observed that all the involved reactions are governed by acidity and basicity. Mixed oxide catalysts derived from layered double hydroxides are therefore promising catalysts for these reactions because their acid/basic properties can be easily adjusted and controlled by varying their elemental compositions.

Layered double hydroxides (LDHs) are a class of two-dimensional anionic clay materials whose general formula is $[M_{1-x}^{2+}M_x^{3+}(OH)_2]^{x+}[A_{x/n}^{n-}nH_2O]_{x-}$ where $M^{2+}$ and $M^{3+}$ are divalent and trivalent metal ions, respectively, and $A^{n-}$ is an anion, e.g. hydrotalcite ($[Mg_3Al(OH)_8][(CO_3)_{1/2}\cdot 2H_2O]$). LDHs are conventionally

* Corresponding author at: The Petroleum and Petrochemical College, Chulalongkorn University, Phayathai Rd. 254, 10330, Bangkok, Thailand.
*E-mail address:* sirirat.j@chula.ac.th (S. Jitkarnka).

https://doi.org/10.1016/j.apcatb.2018.10.073
Received 27 June 2018; Received in revised form 4 October 2018; Accepted 28 October 2018
Available online 30 October 2018
0926-3373/ 

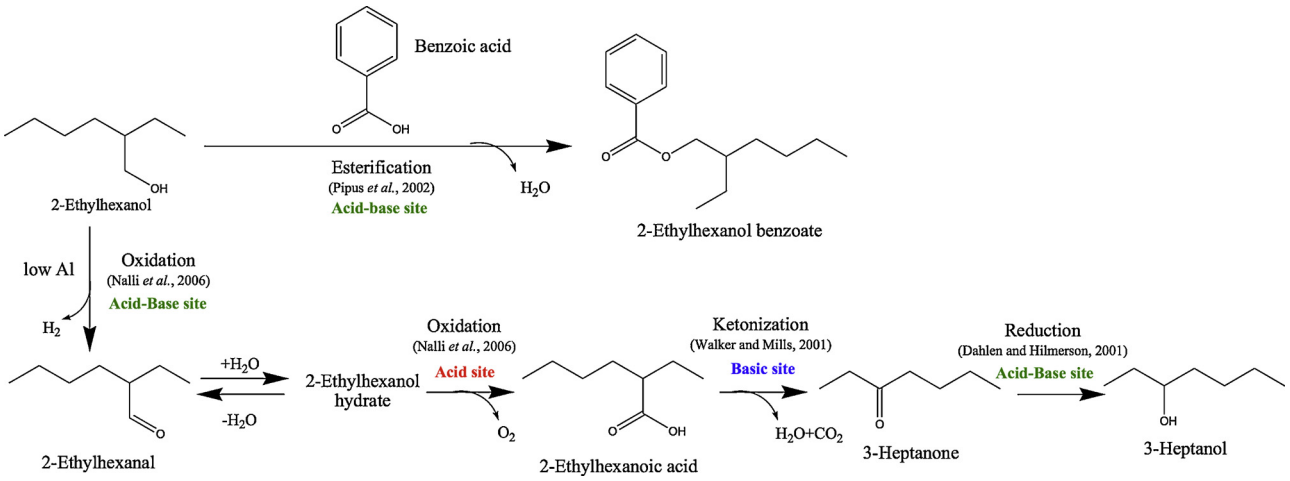


**Scheme 1.** Reaction pathways of benzoic esterification with 2-ethylhexanol [1,9–18].

synthesized using co-precipitation method. However, a new synthesis method using co-precipitation followed by treatment with an aqueous miscible organic (AMO) solvent has been developed to improve the properties of the materials. The AMO-LDHs exhibited significantly high surface area with mesoporosity and specific acid-base properties [19,20]. Generally, when LDHs are calcined, the layered double oxides (LDOs) are formed as mixed oxides that have three active sites: (i) the weak Brønsted basic sites ($OH^-$ groups on the surface), (ii) the medium strength sites Lewis sites (both $Mg^{2+}-O^{2-}$ and $Al^{3+}-O^{2-}$ acid-base pairs), and (iii) the strong Lewis basic sites ($O^{2-}$ anions) [21,22]. Thus, LDOs are able to catalyze a variety of acid-base reactions, such as transesterification and esterification [1,23,24], Knoevenagel condensations [25], and aldol Claisen–Schmidt condensations [26]. The acid-base properties of Mg/Al mixed oxides are generally known to be important for catalytic activity and selectivity, which strongly depend on their chemical composition [12,21,26–28]. However, the correlation between acid-base properties and the bonded atoms of Mg/Al LDOs has not been yet reported to clearly explain in relation with the catalytic activity any of those the reactions. Normally, the structure and bonding atoms are often characterized by using X-ray Absorption Spectroscopy (XAS) that reveals the layered structure, particularly the cation coordination environments [29–32]. The coordination number and interatomic distances of an absorbing atoms around a center atom can be calculated using X-ray Absorption Near Edge Structure (XANES) spectra. Moreover, the phase compositions of catalysts can be determined from Linear combination fitting (LCF) using Extended X-Ray Absorption Fine Structure (XANES) spectra.

This study focused on structure determination and explanation of the acid-basic properties of AMO LDH-based Mg/Al mixed oxides using XANES and EXAFS with various characterization techniques. The objective was to investigate the functions and the acid-base properties, varied with Mg/Al ratio of the catalysts, that can promote the esterification of benzoic acid with 2-ethylhexanol, which was used as a model reaction in this work, to produce valuable chemicals, especially 2-ethylhexyl benzoate.

## 2. Experimentals

### 2.1. Catalyst preparation

The AMO-LDHs with various Mg/Al ratios were first prepared using co-precipitation and Aqueous Miscible Organic Solvent Treatment method [19]. The solutions of $Mg(NO_3)_2.6H_2O$ and $Al(NO_3)_3.9H_2O$ were mixed thoroughly at different Mg/Al ratios of 2.0, 3.0, 4.0, and 5.0 until homogeneity. Then, a $Na_2CO_3$ solution was mixed in the solutions at a specific pH of 10, followed by washing with water and a solvent, and then drying overnight. The AMO-Mg/Al layered double hydroxide (AMO-LDH) samples were named as AMO-$Mg_xAl-CO_3$, where x is 2.0, 3.0, 4.0, and 5.0. The LDHs were calcined at 500 °C in air before uses. The calcined catalysts were named as $Mg_xAlO$, where x is 2.0, 3.0, 4.0, and 5.0.

### 2.2. Catalyst characterization

The concentrations of Mg and Al elements in a solid sample were determined using Inductively Coupled Plasma Optical Emission Spectrometer (ICP), Perkin Elmer, Optima 4300 DV model. The specific surface area, total pore volume, and pore size of a catalyst were obtained from the 27-point nitrogen adsorption and desorption isotherm plots using the Brunauer-Emmett-Teller (BET) technique, Surface Area Analyzer (Quantachrome, Autosorb-1MP). The samples were initially outgassed under vacuum at 250 °C at least 18 h prior to analysis steps. The X-Ray diffraction (XRD) patterns of samples were obtained using X-Ray diffractometer system (Rigaku SmartLab) equipped with a 2.2 kW Cu anode long fine focus ceramic X-ray tube for generating a $CuK_\alpha$ radiation (1.5405 Å). The data were collected in the 2θ range of 5°–70° and scan speed of 0.02° (2θ)/ 0.6 s. The thermal decomposition behavior of an LDH was performed using simultaneous thermogravimetry and differential thermal analysis (TG-DTA), NETZSCH STA 449F3. Under air flow, a sample was heated from 30 °C to 900 °C with a heating rate of 10 °C/min. The acidity and basicity properties of a calcined catalyst were determined from its ability on the temperature programmed desorption of $NH_3$ (TPD-$NH_3$) and $CO_2$ (TPD-$CO_2$) using the Temperature Programmed Desorption/Reduction/Oxidation Analyzer (TPDRO), TPDRO Analyzer, BELCAT II. A sample (50 mg) was pretreated in He (50 cc/min) at 450 °C for 60 min in the machine. For only MgO, the sample size was 500 mg due to its relatively low surface area. Temperature-programmed desorption started with pre-adsorption in 10.03% $NH_3$/He or 99.995 $CO_2$ at 100 °C for 30 min. Then, the temperature was ramped from 100 to 950 °C, 10 °C/min, and held for 30 min with He (30 cc/min). Finally, the acidity or basicity was calculated from the peak area under the TPD profiles.

X-Ray Photoelectron spectroscopy (XPS) was carried out using the AXIS ULTRA$^{DLD}$ XPS machine to determine the oxidation state of elements in samples. The system was equipped with a monochromatic Al X-ray source and a hemispherical analyzer. The spectrometer was operated with the pass energy of 160 eV and 40 eV while wide scan and core level spectra were being recorded. All peaks were calibrated against C1s spectra located at 284.8 eV. X-ray absorption spectroscopy (XAS), including X-ray Absorption Near Edge Structure (XANES) and Extended X-Ray Absorption Fine Structure (EXAFS), were used to investigate the local structure of samples. XAS Spectra were recorded in

transmission mode at room temperature for the Mg and Al K-edges using Beryl (1010) and KTP (1010) crystals, respectively, at Beamline 8 of the Siam Photon Laboratory, Synchrotron Light Research Institute (SLRI), Thailand, with the provided electron beam energy of 1.2 GeV and beam current of 120-80 mA. The X-ray absorption data were processed using the ATHENA and ARTEMIS programs. The composition of a catalyst was determined from Linear combination fitting (LCF) available in the ATHENA program with using the reference spectra of known compounds; that are, MgO (Alfa Aesar, 99.95%), $Mg(OH)_2$ (HIMEDIA, 95%), $MgCO_3$ (HIMEDIA, 60%), $Al_2O_3$ (Sigma-Aldrich, pore size 58 Å), $Al(OH)_3$ (HIMEDIA, 50%), and $MgAl_2O_4$ spinel (Sigma-Aldrich, nanopowder < 50 nm). From the EXAFS spectra, the number and the type of atoms around a central absorbing atom was processed in the ARTEMIS program.

### 2.3. Catalyst activity testing

The catalytic activity was tested in a three-neck round bottom flask reactor, which was equipped with a condenser with Dean–Stark trap and immersed in a heating mantle. In the typical reaction, benzoic acid and 2-ethylhexanol at the initial weight ratio of 1:5.6 were first added to the flask with a catalyst loaded at 10%w/w (weight of catalyst/weight of acid). Then, the mixture was heated to and maintained at 110 °C under continuous stirring with 800 rpm stirring speed. The progress of reaction was monitored by the detection of collected water in the Dean–Stark trap. After the reaction, the catalyst was removed from the reaction mixture using a filter, and the product was analyzed using a gas chromatograph equipped with a Mass Spectrometry of Time of Flight type (GC-TOF/MS), Pegasus LECO GC-TOF/MS. The column, an Rxi-PAH (60 m × 0.25 mm ID and 0.10 µm film thicknesses), was initially set at 40 °C, kept for 1 min, and then increased by 10 °C/min to 210 °C, with the split ratio at 1:50. Initially, the analysis was performed at the injector temperature of 280 °C, with Helium gas at the flowrate of 1.0 ml/min as the carrier gas. The LECO Chroma TOF® software was used to record, analyze, and identify the spectra using the Mass spectrometry library (NIST, Wiley). The reaction was also performed without a catalyst. The benzoic acid conversion, product selectivity, and yields were calculated using Eqs. (1)–(3), respectively.

$$Benzoic\ \ Conversion\ \ (\%) = \frac{[Conc.\ \ of\ \ Benzoic_{inlet} - Conc.\ \ of\ \ Benzoic_{outlet}]}{Conc.\ \ of\ \ Benzoic_{inlet}} \times 100 \quad (1)$$

$$Selectivity\ \ _i(\%) = \frac{Concentration_i\ (wt\%)}{\sum_i^n Concentration_i\,(wt\%)} \times 100 \quad (2)$$

$$Yield_i\ (\%) = \frac{Benzoic\ \ acid\ \ conversion\ \ (\%) \times\ \ Selectivity_i(\%)}{100} \quad (3)$$

;where $i$ is a product, and Conc. is concentration (%wt.).

## 3. Results and discussion

### 3.1. Physical properties

Prior to uses, the synthesis of AMO-$Mg_xAl$-$CO_3$ LDHs was proven successful using the results from characterization. The XRD patterns of AMO-$Mg_xAl$-$CO_3$ LDHs in Fig. 1a show the characteristic peaks of a hydrotalcite; that are, the sharp and intense (003), (006), (009), (015), (018), (110), and (113) reflections at 2θ = 11.50°, 22.90°, 34.74°, 39.13°, 46.28°, 60.46°, and 61.80° (JCPDF No. 00-014-0191). Moreover, the peak of Brucite, $MgOH_2$, located at 2θ = 38.27° and 62.26°, can be detected. It is noted that all the $Mg_xAl$-$CO_3$ samples were successfully synthesized in this work. After calcination at 500 °C, the peaks of periclase (MgO) appear 2θ = 38.27° and 62.26° (JCPDF No.00-001-1235) together with $MgAl_2O_4$ spinel (2θ = 44.45°, JCPDF No.01-075-4038) in the XRD patterns of AMO-$Mg_xAlO$ catalysts (Fig. 1b). The chemical composition, d-spacing, and %weight loss of AMO-$Mg_xAl$-$CO_3$ LDHs are shown in Table 1. From the ICP results, the Mg/Al ratio are closed to the expected ratios, indicating that all the $Mg_xAl$-$CO_3$ LDHs were successfully synthesized in all ratios. Moreover, it is evident that the increasing ratio of Mg in the sheets results in the slight expansion of d-spacing from 7.67 to 7.85 Å, as shown in Fig. 2, since the ionic radius for $Mg^{2+}$ (0.065 nm) is larger than that for $Al^{3+}$ (0.050 nm) [33],

The thermal stability of $Mg_xAl$-$CO_3$ LDHs can be discussed using TGA/DTG profiles, in Fig. 3, which show two distinct regions over the temperature range of 50–260 and 260–900 °C. In the first stage, the loss of water molecules in the interlayer occurs at 50–260 °C [12]. In the second stage, the loss that occurs at 260–400 °C is contributed from the decomposition of carbonate and dehydroxylation in the interlayer [12]. As confirmed by the XRD and TGA results, it is noted that the layered structure has been collapsed, and starts to transform to amorphous mixed oxides (MgO, $Al_2O_3$, and Mg—O—Al) at 500 °C, but the clay sheets are still preserved, as illustrated in Fig. 4. Moreover, at 900 °C, LDHs are totally transformed to mixed oxides. With the increasing Mg/Al molar ratio, the total % weight loss at 900 °C of $Mg_xAl$-$CO_3$ LDH samples increases from 39 to around 43%, as shown in Table 1. The result indicates that a catalyst with a higher Mg/Al ratio has less stable structure. Typically, the layer structure of an Mg—Al LDH can be formed from the substitution of Al atoms in the Mg—O— layered structure, producing a ($[Mg_{1-x}^{2+}Al_x^{3+}(OH)^2]^{x+}$) charge that later coordinates with a carbonate anion during synthesis. It means that when a higher number of Al atoms are inserted into the Mg—O layers, it results in the slightly-higher stability of LDH sheets (as indicated by a lower % weight loss). It can be explained that when a larger number of Al atoms are inserted into the LDH sheets, more cationic sites are created onto the surface of the LDH sheets, and then hooked up with more carbonate anions available during the synthesis, resulting in more stable layered structure of the LDH. In addition, the surface area, mean pore volume, and pore diameter of AMO-$Mg_xAlO$ catalysts are shown in Table 2. The increasing Mg/Al ratio suppresses the surface area and pore volume. With the increasing Mg/Al ratio, the surface area and pore volume decrease to 271.2-207.8 $m^2/g$ and 1.311-0.5156 $cm^3/g$, respectively. The $Mg_2AlO$ catalyst has the highest surface area of 271.2 $m^2/g$ and the pore volume of 1.311 $cm^3/g$. The pore size distribution is shown in Fig. 5, and the average pore diameters were calculated and shown in Table 2. Apparently, all samples are mesoporous materials, as defined by IUPAC [34], because their average pore diameters are in the range of 50–150 Å.

X-Ray Photoelectron spectroscopy (XPS) and X-ray Absorption Near Edge Structure (XANES) were employed to investigate the local structure of samples. The XPS spectra of the reference compounds, $Al_2O_3$ and $MgAl_2O_4$ in Fig. 6a, are employed to confirm $Al^{3+}$ in the octahedral position (74.3 eV) [35]. The Al 2p XPS spectra of $Mg_xAlO$ catalysts (Fig. 6a) show two peaks at the binding energies of around 74.3 to 73.8 eV. These peaks are contributed from $Al^{3+}$ atoms in the catalysts, which are present in two configurations; octahedral (74.3 eV) and tetrahedral (73.2 eV) [35,36]. With increasing Mg/Al ratio from 2:1 to 4:1, the binding energy shifts to that of $Al_{Tet}$ whereas in case of $Mg_5AlO$ catalyst, the binding energy shifts to that of $Al_{Oct}$. Nevertheless, for all samples, the binding energy is in between those of the octahedral $Al^{3+}$ and tetrahedral $Al^{3+}$. Moreover, the three peaks in the Al K-edge XANES spectra of $Mg_xAlO$ catalysts presented in Fig. S1a of the Supplementary document against those of the reference compounds correspond to octahedral $Al^{3+}$ (1568 and 1572 eV) [29] and tetrahedral $Al^{3+}$ (1566 eV) coordinations [29] of aluminum with oxygen atoms. So, both octahedrally- and tetrahedrally-positioned of $Al^{3+}$ are present on the surface of the catalysts. The details of the XANES results are presented in Fig. S1 in the Supporting document.

From the Mg 2p XPS spectra in Fig. 6b, it can be observed that for the AMO-$Mg_xAlO$ catalysts at all Mg/Al ratios, the binding energies range between 49.5 and 49.9 eV. Used as references, MgO has two peaks after deconvolution; that are, Mg—O (50.7 eV) and Mg—OH

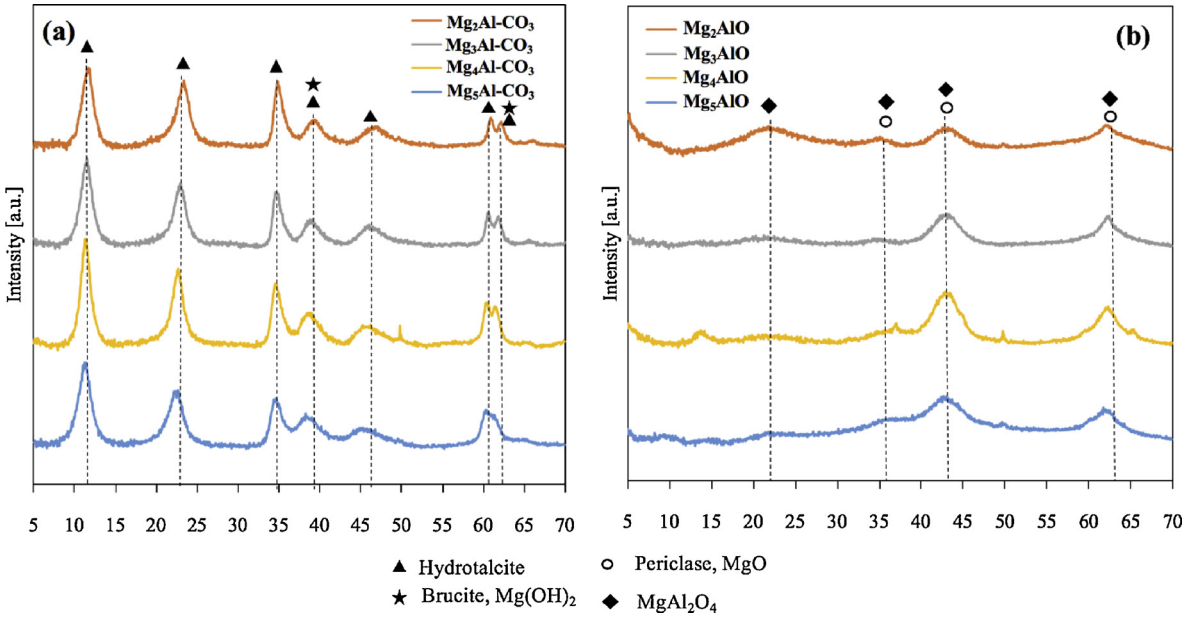


**Fig. 1.** XRD patterns of (a) AMO-$Mg_xAl$-$CO_3$ LDHs and (b) AMO-$Mg_xAlO$ catalysts; ▲Hydrotalcite, ★Brucite ($Mg(OH)_2$), Spinel ($MgAl_2O_4$), and ♦ Periclase (MgO).

**Table 1**
Chemical composition and physical properties of AMO-$Mg_xAl$-$CO_3$ LDHs.

| LDH | Mol Ratio of Mg/Al[a] | Mol %Al[a] | d-Spacing (Å)[b] | % Weight loss[c] at 900 C° |
|---|---|---|---|---|
| $Mg_2Al$-$CO_3$ | 2.08 | 48.1 | 7.67 | 39.0 |
| $Mg_3Al$-$CO_3$ | 3.34 | 29.9 | 7.75 | 40.8 |
| $Mg_4Al$-$CO_3$ | 3.53 | 28.3 | 7.83 | 43.8 |
| $Mg_5Al$-$CO_3$ | 4.43 | 22.6 | 7.85 | 42.8 |

[a] Determined using ICP.
[b] Determined using XRD.
[c] Determined using TGA.

(49.3 eV) in the spectrum, whereas $MgAl_2O_4$ has one peak of Mg—O—Al (50.2 eV) [37]. Therefore, the Mg 2p binding energies of $Mg_xAlO$ catalysts are found in the neighborhood of those of Mg—O, Mg—O—Al, and Mg—OH. As the Mg/Al ratio is increased from 2:1 to 3:1, the peak of Mg shifts to a lower binding energy, inferring the decrease in oxidation state of Mg, which indicates the emerging of Mg—OH phase. On the other hand, at the ratio of 5:1, the peak of Mg shifts to a higher binding energy (49.8 eV) toward those of the Mg—O—Al and Mg—O phases. Furthermore, according to the analysis of Mg K-edge XANES spectra shown in the Supplementary document, it is evident that the spectra of AMO-$Mg_xAlO$ catalysts are quite similar to that of MgO standard spectrum. Therefore, the divalent Mg cations in the catalysts are mostly octahedrally coordinated with oxygen atoms. Conclusively, both XPS and XANES analyses suggest that the mixed phases of Mg—O, Mg—Al—O, and Al—O are present in the $Mg_xAlO$ catalysts.

To quantify the phase compositions in the $Mg_xAlO$ catalysts, the Al- and Mg K-edge spectra were fitted with those of standard compounds using Linear Combination Fitting (LCF) tool in the ATHENA program. The phase compositions are shown in Table 3. The Mg K-edge spectra of all samples were fitted with those of $Mg(OH)_2$, $MgAl_2O_4$, and MgO. The increasing Mg/Al ratio changes the relative composition of $Mg(OH)_2$, $MgAl_2O_4$, and MgO phases in the catalysts. The $Mg_2AlO$ and $Mg_3AlO$ catalysts are found to be composed of $Mg(OH)_2$ and $MgAl_2O_4$ phases only. When the Mg/Al ratio increases from 2 to 3, the composition of $Mg(OH)_2$ increases while that of $MgAl_2O_4$ decreases. At the ratio of 4 and 5, the $MgAl_2O_4$ content significantly increases, together with the emerging MgO phase.

Furthermore, the Al K-edge XANES spectra of $Mg_xAlO$ catalysts are fitted with those of $Al(OH)_3$, $MgAl_2O_4$, and $Al_2O_3$ reference standards. Except the $Mg_3AlO$ catalyst, the composition of all catalysts are found to be the mixed phases of $Al(OH)_3$ and $MgAl_2O_4$. It can be inferred that the clay sheet structure does not destroy at calcination at 500 °C because of presence of Al—OH phase. Moreover, excess Mg or Al are aggregated to metal oxide phase (Mg—O—Al) outside the clay sheet, as shown in Fig. 4. These results can be confirmed by XRD and TGA

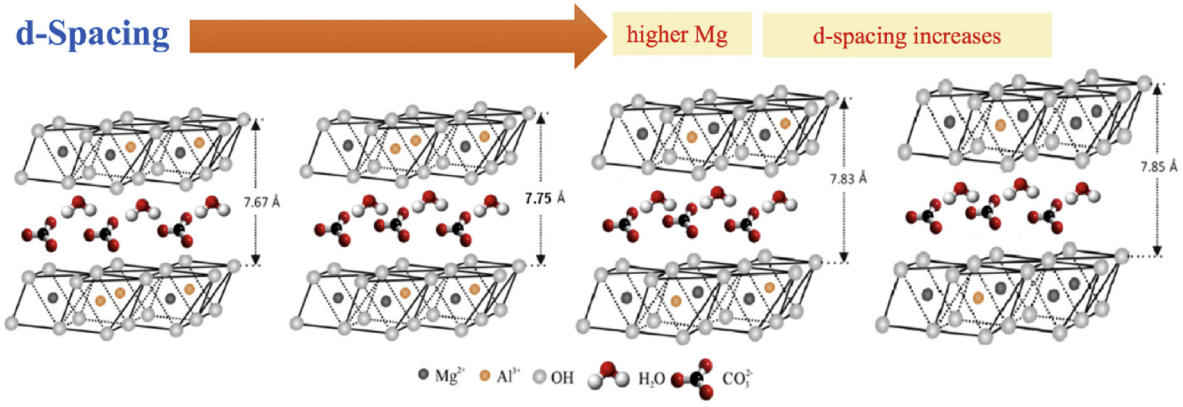


**Fig. 2.** d-spacing of AMO-$Mg_xAl$-$CO_3$ LDHs at various Mg/Al ratios.

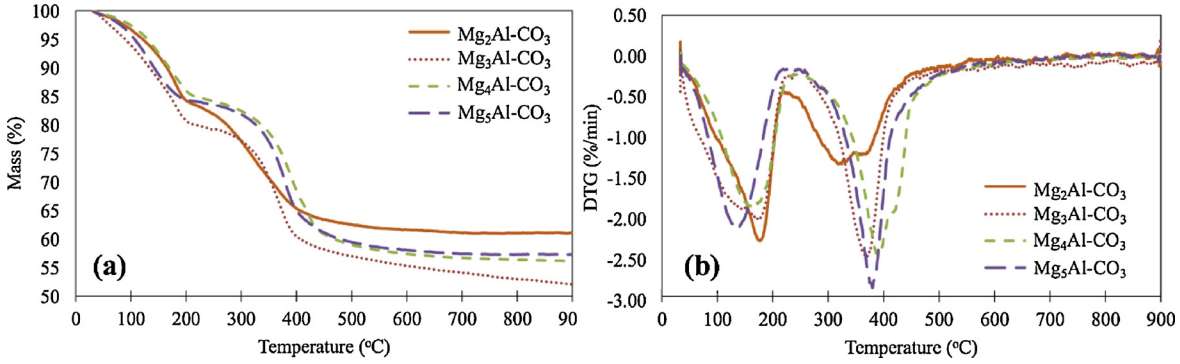


**Fig. 3.** (a) TGA and (b) DTG profiles of AMO-$Mg_xAl$-$CO_3$ LDHs at various Mg/Al ratios.

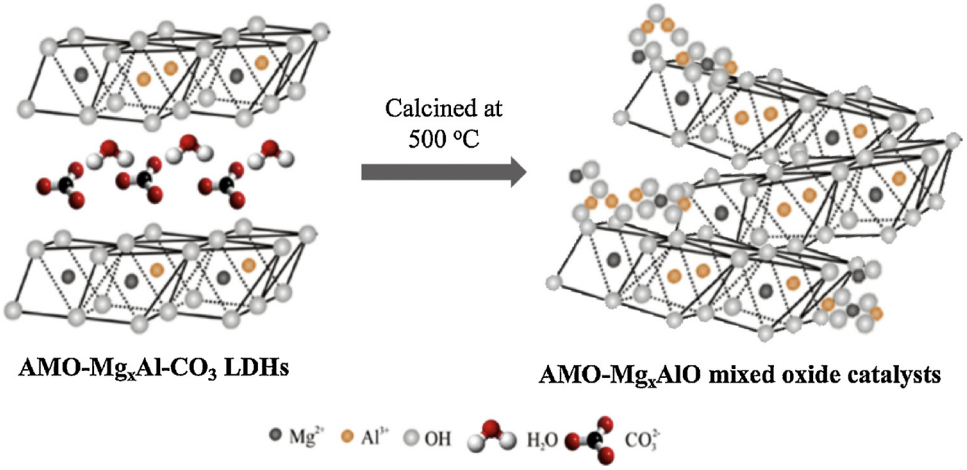


**Fig. 4.** Schematic of the transformation of AMO-$Mg_xAl$-$CO_3$ LDHs to AMO LDH-derived $Mg_xAlO$ catalysts at 500 °C of calcination.

**Table 2**
Physical properties of AMO LDH-derived $Mg_xAlO$ catalysts (the calcined AMO-$Mg_xAl$-$CO_3$ LDHs).

| Catalyst | Surface Area ($m^2$/g)[a] | Pore Volume ($cm^3$/g)[a] | Average Pore Diameter (Å)[a] |
|---|---|---|---|
| $Mg_2AlO$ | 271.2 | 1.311 | 148 |
| $Mg_3AlO$ | 220.9 | 1.294 | 129 |
| $Mg_4AlO$ | 213.9 | 0.4559 | 49.4 |
| $Mg_5AlO$ | 207.8 | 0.5156 | 56.1 |

[a] Determined using BET.

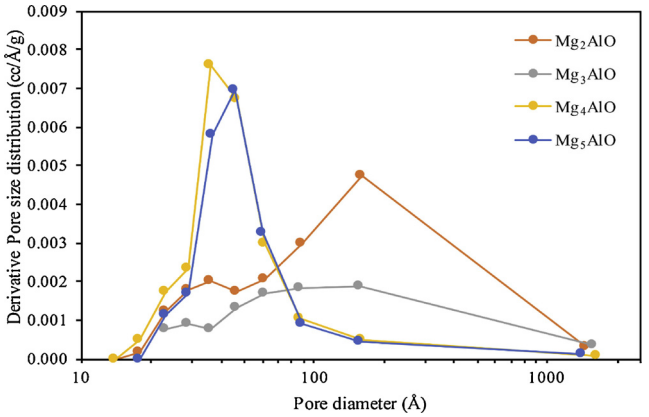


**Fig. 5.** Pore size distributions of AMO-$Mg_xAlO$ catalysts.

analyses. The $Mg_3AlO$ catalyst was derived from the AMO-$Mg_3Al$-$CO_3$ LDH, whose Mg/Al ratio is a suitable ratio of natural anion clay sheets. Thus, when the LDH is calcined at 500 °C, it completely transforms to the mixed oxide in the form of calcined clay sheet structure, which the Al—OH phase is present.

In summary, the coordination of the aluminum atoms was found in both octahedral and tetrahedral configurations, whereas magnesium atoms were found to exist only octahedral configuration. Moreover, different Mg/Al ratios results in the different relative compositions of catalysts; that are, $Mg(OH)_2$, $Al(OH)_3$, $MgAl_2O_4$, and MgO phases.

### 3.2. Acidity and basicity

#### 3.2.1. TPD-$CO_2$ and TPD-$NH_3$

The acid-base properties of AMO LDH-derived $Mg_xAlO$ catalysts obtained from TPD of $CO_2$ and $NH_3$ are shown in Fig. 7 and Table 4, in comparison of those of MgO, $Al_2O_3$, and $MgAl_2O_4$. From the TPD profiles, both acidic and basic sites are found present on the catalysts as illustrated in Fig. 7a and b, respectively. Both acidity and basicity can be depicted from only one big profile ranging from 100 to 450 °C. Likewise, based on previous reports [22,38], the similar TPD-$NH_3$ profiles of conventional LDH-derived $Mg_xAlO$ catalysts were presumably divided into three desorption peaks with different strength; that are, weak acid sites (low-temperature peak, 150–200 °C), medium acid sites (medium-temperature peak, 200–260 °C), and strong acid sites (high-temperature peak, 260–350 °C). However, all the three sites were hardly separated, and cannot be firmly identified to any specific types of acid sites. Nevertheless, the above-mentioned weak and medium acid sites could be the same site, which was confirmed from the IR and calorimetric measurements of the $NH_3$ adsorption [12,39,40]. It was found that the $Mg_xAlO$ catalysts contain merely two

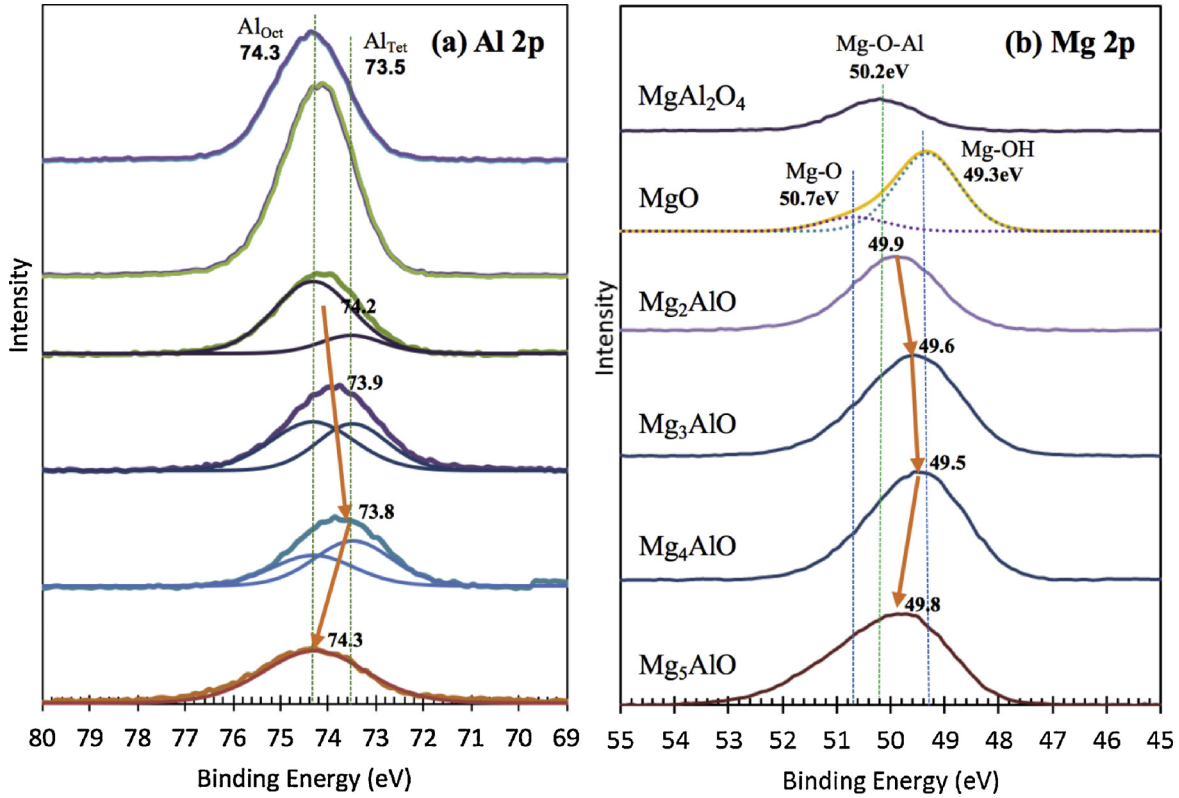


**Fig. 6.** XPS spectra of AMO LDH-derived $Mg_xAlO$ catalysts: (a) Al 2p and (b) Mg 2p.

types of sites; namely, the Brønsted site that is the surface OH group represented by the low-temperature peak at 100–200 °C, and Lewis acid site identified to Al—O—Mg species that give $Al^{3+}—O^{2-}$ sites (high-temperature peak, 200–350 °C). Based on the TPD profiles of this work and the discoveries in previous reports [12,39,40], the AMO-$Mg_xAlO$ catalysts are, thus, considered to possess two types of acid sites; that are, weak acid sites (low-temperature peak, 150–200 °C) and strong acid sites (high-temperature peak, 200–350 °C), which are assigned to Bronsted acid site OH group (Acid Site#1) and Lewis acid sites provided by $Al^{3+}—O^{2-}$ pairs (Acid Site#2), respectively (see Table 4). The illustration of two acid site types of the AMO-$Mg_xAlO$ catalysts can be depicted in Fig. 8a. Hence, as Mg/Al ratio affects the density and strength of acid, it can be observed that the total acid density dramatically decreases, from 0.479 to 0.355 mmol/g, when the Mg/Al ratio is increased from 2 to 5, because of the reducing percentage of Al in the catalysts. With the increasing Mg/Al ratio from 2 to 3, the acid peak shifts to a higher temperature, and then shifts to a lower temperature again with the increasing ratio from 4 to 5, as shown in Fig. 7a, inferring to the change in acid strength. The $Mg_3AlO$ catalyst is therefore found to have the highest acid strength.

The basicity of AMO $Mg_xAlO$ catalysts is also summarized in Table 4, and can also visualized in Fig. 8a. The three types of basic sites have been identified based on the previous reports [12,22,41]. The weak Bronsted basic site (Basic Site #1) is related to $OH^-$ groups on the surface, the medium strength Lewis basic site (Basic Site #2) is associated with oxygen in $Mg^{2+}—O^{2-}$ pairs, whereas the strong Lewis basic site is related to isolated $O^{2-}$ anions (Basic Site #3), as shown in Fig. 8a. As the Mg/Al ratio is increased, the strength of basic site decreased, except at the ratio of 3:1. It is found that $Mg_4AlO$ catalyst has the highest basic strength. In addition, it can be observed that the total basic density decreases, ranging from 0.676 to 0.232 mmol/g, with the increasing Mg/Al ratio.

When the TPD-$NH_3$ and $CO_2$ profiles of the AMO LDH-derived $Mg_xAlO$ catalysts are compared to those of MgO, $Al_2O_3$, and $MgAl_2O_4$ references, it can be observed that the changing acid and basic sites of the catalysts well correlate with the change of their MgO, $Al_2O_3$, and $MgAl_2O_4$ phases. Consequently, it can be assumed that the greatly-changing numbers of acid sites and basic sites may have been contributed from the spinel ($MgAl_2O_4$) phase or a binary mixed oxide that generates acid-base pairs. Moreover, it is suspicious that the changing acid-basic strength may be resulted from the altered coordination number of Al and Mg atoms in the structure, which is next discussed in the EXAFS analysis part.

**Table 3**
Phase compositions in the AMO LDH-derived $Mg_xAlO$ catalysts from Linear Combination Fitting.

| Sample | Mg K-edge | | | | Al K-edge | | | |
|---|---|---|---|---|---|---|---|---|
| | % Composition | | | R factor | % Composition | | | R factor |
| | $Mg(OH)_2$ | $MgAl_2O_4$ | MgO | | $Al(OH)_3$ | $MgAl_2O_4$ | $Al_2O_3$ | |
| $Mg_2AlO$ | 45.0 | 55.0 | 0 | 0.0297 | 88.2 | 11.8 | 0 | 0.0566 |
| $Mg_3AlO$ | 59.4 | 40.6 | 0 | 0.0256 | 100 | 0 | 0 | 0.0545 |
| $Mg_4AlO$ | 33.0 | 50.6 | 16.4 | 0.0228 | 98.2 | 1.80 | 0 | 0.0751 |
| $Mg_5AlO$ | 33.6 | 57.9 | 8.50 | 0.0264 | 81.7 | 18.3 | 0 | 0.0501 |

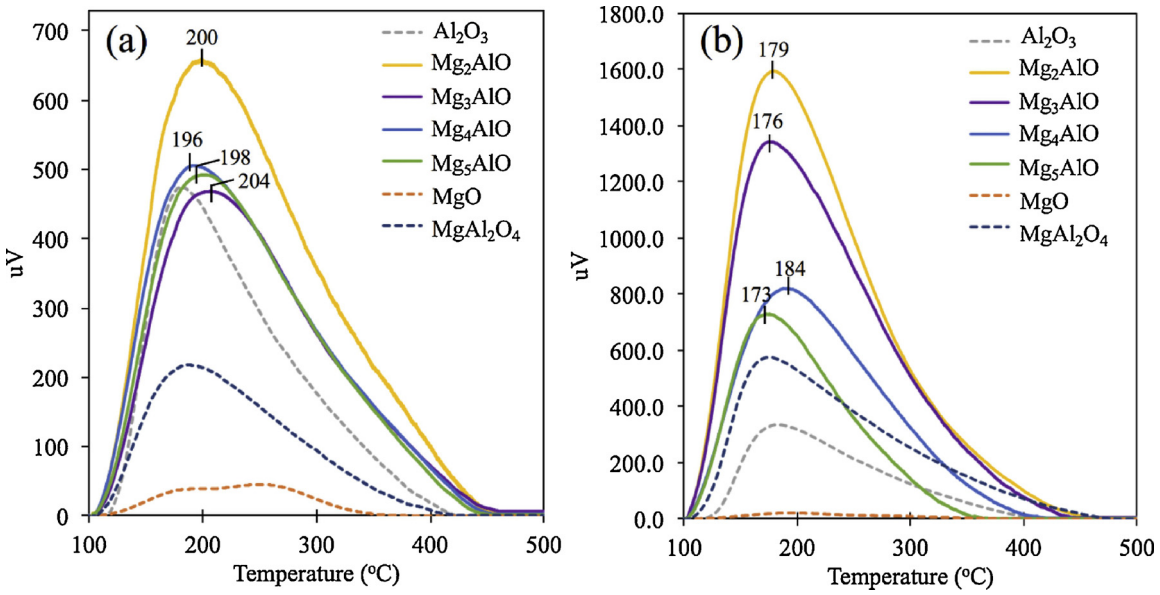


**Fig. 7.** TPD profiles: (a) $NH_3$ (acidity), and (b) $CO_2$ (basicity) of AMO LDH-derived $Mg_xAlO$ catalysts.

### 3.2.2. EXAFS analysis

The radial structure function (RSF) from Fourier Transform of the $k^2$-weighted EXAFS are plotted for the two experimental data and their best fit, in the range of 3–7 $Å^{-1}$ for Mg K-edge and 3–6.5 $Å^{-1}$ for Al K-edge of the catalysts, as shown in Figs. S2 and S3 (in the Supplementary document), respectively. The number and the type of atoms around the central absorbing atom and the local structure from calculated inter-atomic distances (R), coordination numbers (C.N.), and Debye-Waller factors ($\sigma^2$) were determined by a detailed EXAFS data analysis by using the ARTEMIS program. The local structure parameters are presented in Table 5. Previously, the structure of a calcined conventional $Mg_xAl$-LDO material has been proposed on account of the coordination of Mg—O, Al—O, and Mg—O—Al in the structure together with the formation of MgO like phase (octahedral Mg), Mg—OH, Al—OH, and a mixed octahedral/tetrahedral Al phase [29,42]. Since the AMO-$Mg_xAlO$ catalysts in this work contain the similar phase compositions, their structures can be drawn similarly with the new information from characterization of the unique AMO materials. As a result, the structures of AMO-$Mg_xAlO$ catalysts at various Mg/Al ratios and the locations of Mg and Al cations with coordination, drawn from EXAFS and XANES data, can be illustrated in Fig. 8b. It can be seen that the coordination number (C.N.) and atomic distances (R) of AMO-$Mg_xAlO$ materials change upon the Mg/Al ratio.

For the $Mg_2AlO$ catalyst, the coordination number (C.N.) around the cations (Mg—O and Al—O) is approximately six atoms (Table 4). Moreover, the XANES data of $Mg_2AlO$ (Table 3) indicate the existence of only Mg—OH and Al—OH phases; thus, the OH groups are possibly attached to the Mg and Al atoms in the structure. With the increasing Mg/Al ratio to 3, it can be seen that the C.N. of Mg—O (5.7) is similar to that of the C.N. of Mg—O in $Mg_2AlO$, whereas the C.N. of Al—O (7.1) is higher than those of the other catalysts. The numbers of oxygen around the Al atom is seven atoms, which is possible to be the OH group since only Al—OH phase is found in the $Mg_2AlO$ catalyst (Table 3). When the Mg/Al ratio increases from 3 to 5, the C.N. of Al—O ranges from 5.6 to 5.9, which is similar to that of the $Mg_2AlO$ catalyst. However, the C.N. of Mg-Mg (C.N. = 9.4–10.0) and Mg—O (C.N. = 6.7–6.6) of the $Mg_4AlO$ and $Mg_5AlO$ catalysts are higher because the formation of MgO phase is observed (XANEs data, Table 3). Additionally, the bond distances (R) at the Mg/Al ratios of 2 and 4 are similar; that are, Mg—O ($R \approx 2.08$), Mg—Mg ($R \approx 2.9$), and Mg—Al ($R \approx 2.9$). Likewise, the catalysts with the Mg/Al ratios of 3 and 5 have the similar bond distances of Mg—O ($R \approx 2.01$), Mg-Mg ($R \approx 3.4$), and Mg—Al ($R \approx 2.8$).

From the Al K-edge data, with the increasing Mg/Al ratio, the bond distance of Al—O ranges from 1.92 to 1.93, except the $Mg_3AlO$ catalyst that has the bond distance of 1.96 with the higher C.N. of Al—O (7.1). Such a higher C.N. could reduce the charge density around the Al

**Table 4**
Acid-base properties of AMO LDH-derived $Mg_xAlO$ catalysts.

| Catalyst | Density of acid (mmol/g)[a] | | | Density of basic (mmol/g)[b] | | | | Ratio of Acid/Base density |
|---|---|---|---|---|---|---|---|---|
| | Acid site#1[c] | Acid site#2[d, e] | Total Acidity | Basic site#1[c] | Basic site#2[d] | Basic site#3[e] | Total basicity | |
| $Mg_2AlO$ | 0.158 | 0.321 | 0.479 | 0.211 | 0.274 | 0.191 | 0.676 | 0.71 |
| $Mg_3AlO$ | 0.115 | 0.257 | 0.372 | 0.189 | 0.158 | 0.240 | 0.587 | 0.63 |
| $Mg_4AlO$ | 0.114 | 0.266 | 0.380 | 0.170 | 0.118 | 0.063 | 0.351 | 1.08 |
| $Mg_5AlO$ | 0.119 | 0.236 | 0.355 | 0.083 | 0.085 | 0.064 | 0.232 | 1.53 |
| $Al_2O_3$ | 0.072 | 0.200 | 0.272 | 0.026 | 0.045 | 0.051 | 0.122 | 2.23 |
| MgO | 0.001 | 0.002 | 0.003 | 0.020 | 0.015 | – | 0.035 | 0.09 |
| $MgAl_2O_4$ | 0.030 | 0.109 | 0.139 | 0.057 | 0.090 | 0.108 | 0.255 | 0.55 |

[a] Determined using TPD-$NH_3$.
[b] Determined using TPD-$CO_2$.
[c] Low-temperature peak.
[d] Medium-temperature peak.
[e] High-temperature peak (260–350 °C).

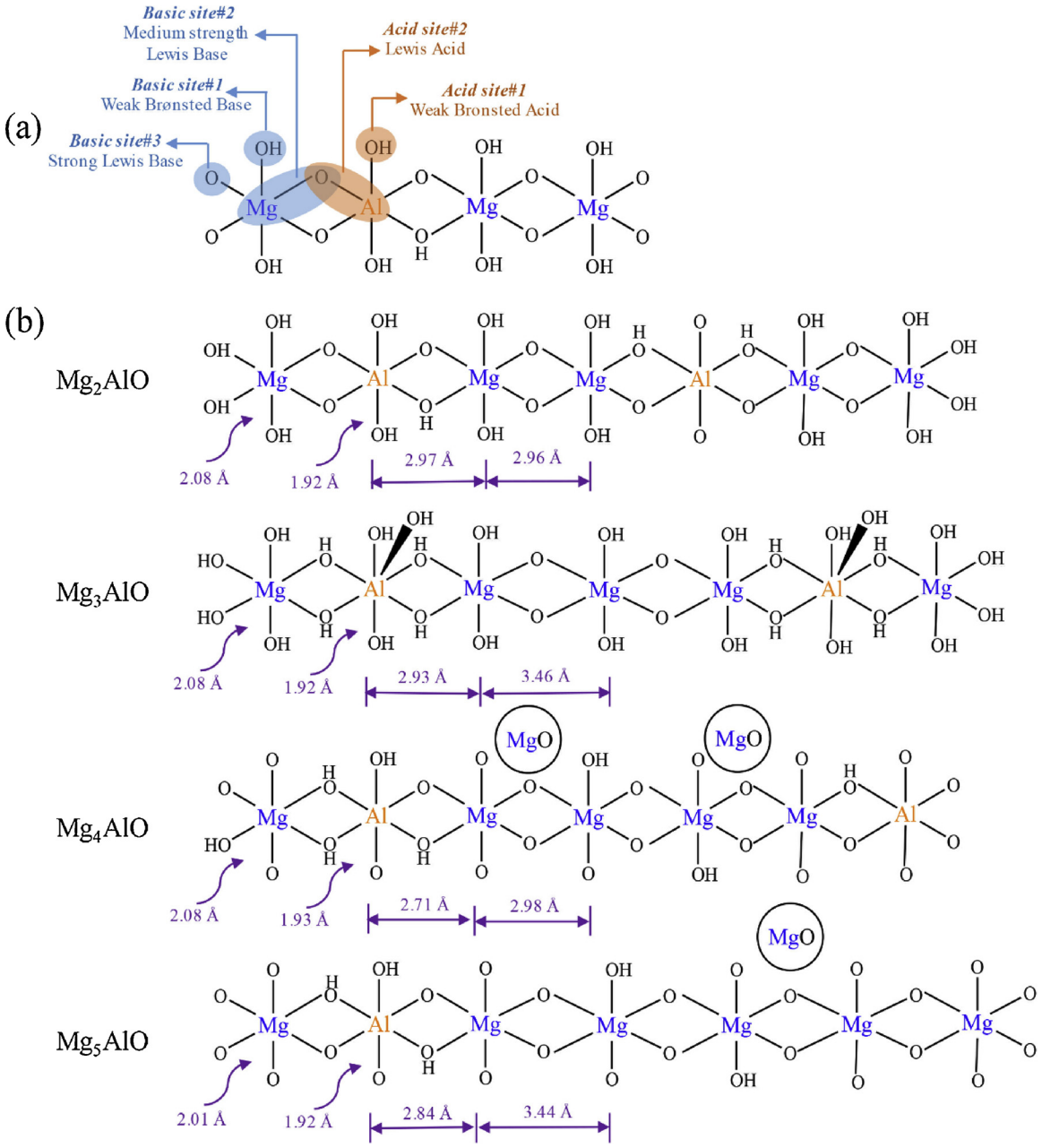


**Fig. 8.** (a) Illustration of the acid and base sites of AMO-$Mg_xAlO$ catalysts, and (b) Structure changes with increasing Mg/Al ratio derived from XANES and EXAFS analysis.

atoms, when compared to that of Al atoms with a lower C.N. Moreover, the distortion of the angle between the Mg—O—Al in the structure is associated with the bond distance between Mg—Al. Hence, the Mg/Al ratio has the impact also on the enlargement of Mg—Al bond distance, not only the coordination number. Therefore, the acid-base properties of the AMO $Mg_xAlO$ catalysts can be explained using the structures in Fig. 8b. The substitution of $Al^{3+}$ into $Mg^{2+}$ structure, forming Al—O bonds, produces a cationic site that behaves as acid sites (Acid Sites #1 and #2). Moreover, the acid strength is found to be related with the C.N. of Al—O bond since it is found that the acid strength of the $Mg_3AlO$ catalyst is the highest, followed by that of $Mg_2AlO$ > $Mg_5AlO$ > $Mg_4AlO$ (Fig. 7a), which is in the same order of the C.N. of Al—O bond. Moreover, more distributed $Al(OH)_3$ phase containing more Al—OH bonds is highly found in the $Mg_3AlO$ catalyst in association with a higher C.N. that results in the lower charge density around the Al atoms; thus, the acid strength these OH bonds around the Al atoms is stronger since $H^+$ is more easily given. In addition, the Mg—O—Al and Mg—O bonds, formed from the substitution of $Al^{3+}$ in the sheets, bring about the formation of acid and strong basic sites on the surface of mixed oxide. Namely, the $O^{2-}$ anions adjacent to the $Mg^{2+}$ or $Al^{3+}$ become coordinatively unsaturated, forming strong basic sites (Basic site #3) [12]. Hence, the basic strength depends on the oxygen around both Mg—O and Mg—O—Al bonds. Interestingly, the highest basic strength is observed in the $Mg_4AlO$ catalyst that has the highest C.N. of Mg—O (C.N. = 6.7) and the high content of $MgAl_2O_4$ (50.6%, Table 3) and MgO (16.4%, Table 3). In summary, the $Mg_xAlO$ catalysts possess both acidic and basic sites the acid-base pairs ($Mg^{2+}$—$O^{2-}$ and $Al^{3+}$—$O^2$ pairs) with varying densities and strengths, depending on the phases that are formed during calcination.

**Table 5**
Structural parameters from the Al K-edge and Mg K-edge EXAFS spectra for the AMO LDH-derived $Mg_xAlO$ catalysts.

| Sample | Mg K-edge | | | | | | Al K-edge | | | | | |
|---|---|---|---|---|---|---|---|---|---|---|---|---|
| | Bond type | C.N.[a] | R (Å)[b] | ΔE° (eV)[c] | $\sigma^2$ ($10^{-3}$, Å$^2$)[d] | R factor | Bond type | C.N.[a] | R (Å)[b] | ΔE° (eV)[c] | $\sigma^2$ ($10^{-3}$, Å$^2$)[d] | R factor |
| **$Mg_2AlO$** | **Mg—O** | 5.5 ± (0.7) | 2.08 | 7.02 | 1.0 | 0.0337 | **Al—O** | 5.9 ± (0.6) | 1.92 | 9.80 | 2.1 | 0.0229 |
| | **Mg—Mg** | 4.5 ± (1.9) | 2.96 | | 1.8 | | | | | | | |
| | **Mg—Al** | 1.8 ± (1.9) | 2.97 | | 1.8 | | | | | | | |
| **$Mg_3AlO$** | **Mg—O** | 5.7 ± (0.6) | 2.01 | −0.21 | 11.7 | 0.0200 | **Al—O** | 7.1 ± (0.9) | 1.96 | 9.13 | 2.0 | 0.0366 |
| | **Mg—Mg** | 3.5 ± (1.0) | 3.46 | | 2.8 | | | | | | | |
| | **Mg—Al** | 1.3 ± (0.3) | 2.93 | | 2.8 | | | | | | | |
| **$Mg_4AlO$** | **Mg—O** | 6.7 ± (0.8) | 2.08 | −0.50 | 5.0 | 0.0213 | **Al—O** | 5.6 ± (0.7) | 1.93 | 9.14 | 0.9 | 0.0355 |
| | **Mg—Mg** | 9.4 ± (1.3) | 2.98 | | 0.11 | | | | | | | |
| | **Mg—Al** | 1.7 ± (0.9) | 2.71 | | 0.07 | | | | | | | |
| **$Mg_5AlO$** | **Mg—O** | 6.6 ± (1.1) | 2.01 | −1.86 | 5.4 | 0.0292 | **Al—O** | 5.8 ± (1.1) | 1.92 | 8.53 | 4.2 | 0.0380 |
| | **Mg—Mg** | 10.0 ± (3.0) | 3.44 | | 0.01 | | | | | | | |
| | **Mg—Al** | 3.0 ± (1.6) | 2.84 | | 0.01 | | | | | | | |

[a] Coordination number.
[b] Distance.
[c] Threshold energy difference.
[d] Debye-Waller factor.

### 3.3. Catalytic activity

The AMO LDH-derived $Mg_xAlO$ catalysts were tested for their activity on esterification of benzoic acid with 2-ethylhexanol to 2-ethylhexyl benzoate. The conversion of benzoic acid is shown in Fig. 9. At the time-on-stream 10 h, bulk MgO and $Al_2O_3$ give only 15.8% and 13.4% conversion, respectively, whereas all AMO-catalysts enhances the conversion of benzoic acid to 40.7–66.1%. The catalyst with Mg/Al ratio of 4:1 gave the highest benzoic conversion of 66.1% whereas the $Mg_3AlO$ one gives the lowest conversion among the other catalysts. It is found that the conversion of benzoic acid correlates with the acid-base pair sites; namely, it increases with the ratio of acid/base density (Table 4). Moreover, the AMO-$Mg_xAlO$ catalysts give far better benzoic acid conversion than an individual oxide (MgO and $Al_2O_3$) because they contain the active Mg—O—Al phase that creates the Lewis acid-base pairs ($Mg^{2+}$—$O^{2-}$ and $Al^{3+}$—$O^{2-}$ pairs) and basic sites ($O^{2-}$ anions), which are needed to activate the reactant and drive the esterification reaction [12]. The activation of benzoic acid and 2-ethylhexanol, followed by the esterification reaction and then the formation of 2-ethylhexyl benzoate, on the AMO-$Mg_xAlO$ catalysts can be postulated as illustrated in Fig. 10(a1). First, benzoic acid and 2-ethylhexanol are simultaneously activated on separate sites; that are, the Lewis acid site ($Al^{3+}$—$O^{2-}$) and basic sites ($O^{2-}$ anions), respectively. Namely, benzoic acid is pre-adsorbed on $Al^{3+}$—$O^{2-}$ of the catalyst surface. Then, the $Al^{3+}$ site interacts with the nonligand electrons of oxygen atoms in the carbonyl group of benzoic acid, and gives electrophilic (positive charge) over carbonyl carbon. Simultaneously, 2-ethylhexanol is adsorbed through the O—H bond on $O^{2-}$ anion (basic sites) on the catalysts. Then, the reaction of 2-ethylhexanol with benzoic acid occurs from the nucleophilic attack onto the carbonyl site, which leads to the formation of an oxonium ion, and then the subsequent deprotonation, followed by the desorption of product intermediate, finally releasing 2-ethylhexyl benzoate and water molecule, as the products. Moreover, the hydroxyl group on the surface (Mg(Al)—OH phase) also can promote the esterification reaction due to the relatively-high electronegativity of metal ion [43], as shown in Fig. 10(a2). The proton of hydroxyl group can attack an oxygen atom in carbonyl group of benzoic acid, which leads to an electrophilic carbon of carbonyl group. Then, the coordination of 2-ethylhexanol with benzoic acid takes place on the surface, finally forming 2-ethylhexyl benzoate and water molecule. However, the conversion of benzoic acid does not only depend on the acid-base pair density, but also the acid-base strength that affects the adsorption of reactants on the acid-base sites of catalysts. It can be observed that the catalyst that possesses a lower ratio of total acid/base density (see Table 4), is likely to give a higher conversion of benzoic acid, except the $Mg_3AlO$ catalyst that has the lowest ratio of total acid/base density gives the lowest conversion of benzoic acid. However, the $Mg_3AlO$ catalyst has the highest acid strength. Therefore, it can be explained that although the $Mg_3AlO$ catalyst has a lower ratio of total acid/base density than any of the other three catalysts, its strength is too strong that benzoic acid can be strongly adsorbed, but rarely be converted. Thus, only suitable acid-base strength would allow the adsorption of reactants to occur, then the reaction to take place, and the products to be formed.

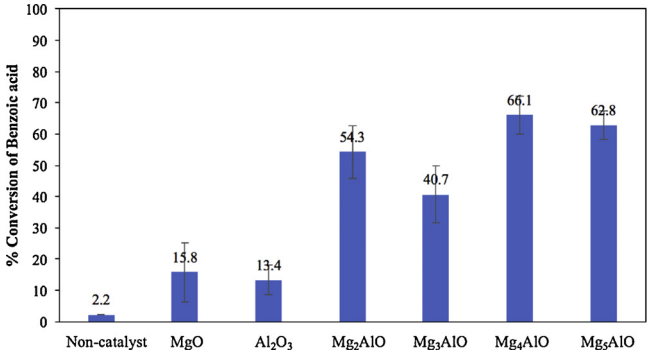


**Fig. 9.** Conversion of benzoic acid using the AMO-$Mg_xAlO$ catalysts at various Mg/Al ratios.

Fig. 11 exhibits all products that consist of 2-ethylhexyl benzoate, 2-ethylhexanal, 3-heptanone and 3-heptanol as similar as collected from various sources and shown in the general reaction pathways (Scheme 1). The non-catalytic case, $Al_2O_3$, MgO, and the AMO-$Mg_2AlO$ catalyst produce only 2-ethylhexylbenzoate, indicating that only the esterification pathway is driven. For the other AMO-$Mg_xAlO$ catalysts, the oxidation of 2-ethylhexanol to 2-ethylhexanoic acid followed by ketonization, which result in 2-ethylhexanal, 3-heptanone, and 3-heptanol, simultaneously take place. When the Mg/Al ratio increases from 3 to 5, the selectivity of 2-ethylhexanal is enhanced to 22–40 wt%. Moreover, the AMO-based catalysts with the Mg/Al ratio of 3 to 4 can produce 6–16% 3-heptanone and 2–5% 3-heptanol.

Unlike the other AMO-based catalysts, the $Mg_2AlO$ catalyst gives 100% selectivity of 2-ethylhexyl benzoate. Interestingly, it is worthy noted that the $Mg_2AlO$ catalyst that has the highest % Al content (Table 1) does not promote the oxidation of 2-ethylxanol. However, the increasing concentration of Mg in the catalysts can cause the formation of 2-ethylhexanal, which is an undesired product, indicating that Mg

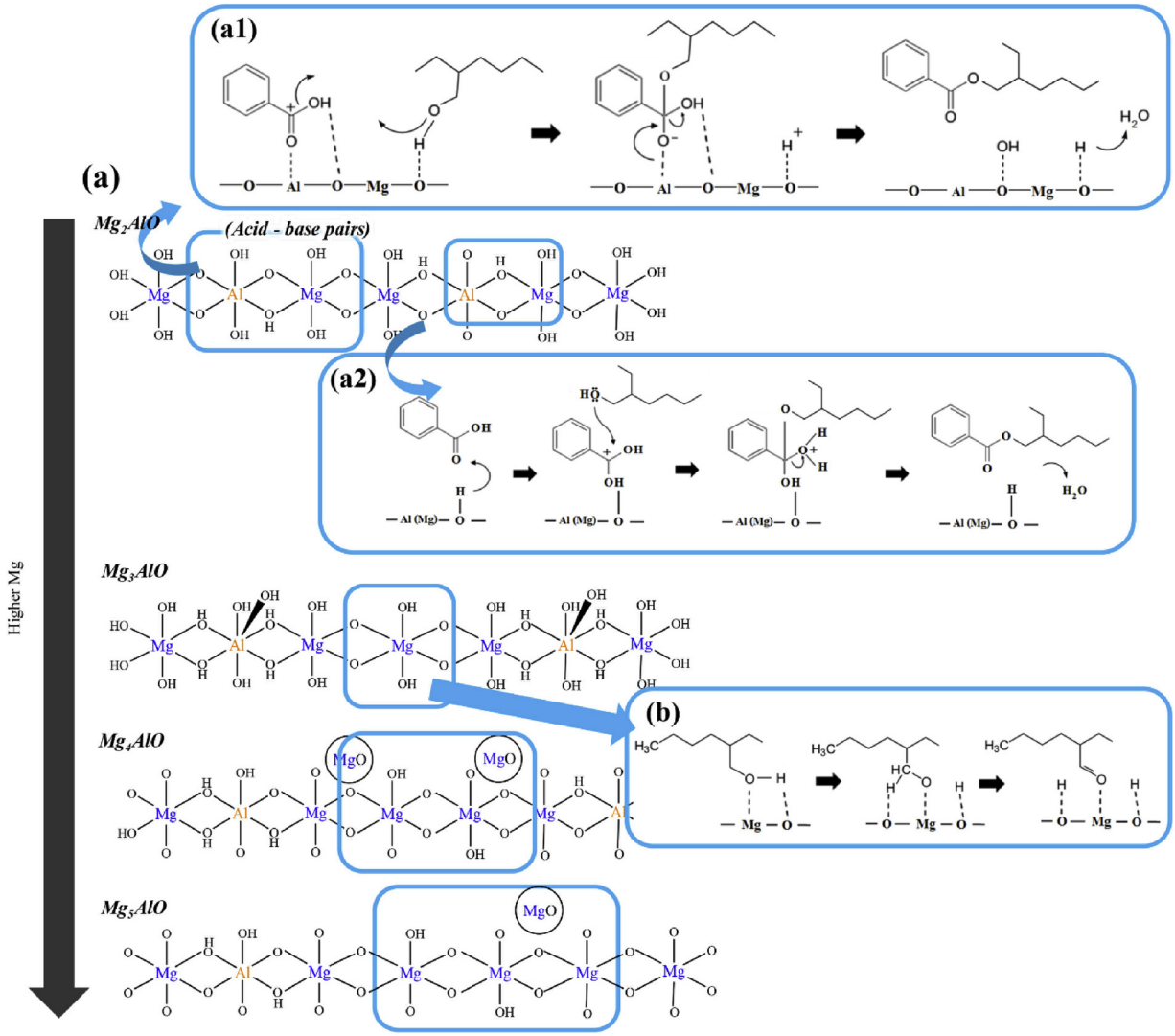


**Fig. 10.** (a) Proposed mechanism for esterification of benzoic acid with 2-ethylhexanol over (a1) AMO-$Mg_xAlO$ catalysts (modified from [9]) and (a2) Mg(Al)—OH sites (modified from [38]), and (b) oxidation of 2-ethylhexanol over magnesium sites.

can promote the oxidation of 2-ethylhexanol to 2-ethylhexanal. It is possible that 2-ethylhexanol is preferentially adsorbed on the Mg sites, promoting the oxidation reaction, as illustrated in Fig. 10(b). As the Mg/Al ratio increases, the Mg content in the catalysts increases (low %Al content), and then the oxidation reaction is more likely to occur. Additionally, the $Mg_3AlO$ and $Mg_4AlO$ catalysts can further convert 2-ethylhexanal to 3-heptanone via oxidation and ketonization. As for Mg/Al ratio of 5:1, the $Mg_5AlO$ catalyst cannot drive the oxidation of 2-ethylhexanal, which is governed by basic sites, because of its lowest basic density. So, 3-heptanone and 3-heptanol are not observed from using $Mg_5AlO$ as a catalyst.

To compromise between conversion and selectivity, the product yields are shown in Fig. 12. It is found that the AMO-$Mg_2AlO$ catalyst gives the highest yield of 2-ethylhexyl benzoate since it gives 100% selectivity of 2-ethylhexyl benzoate with a high conversion. So, the $Mg_2AlO$ catalyst performs the most efficiently for the esterification of benzoic acid with 2-ethylhexanol to the 2-ethylhexyl benzoate. Moreover, it is evident that the $Mg_2AlO$ catalyst, which possesses the highest total acid density together with the highest total base density, gives the highest yield of 2-ethylhexyl benzoate, confirming that both acid and base sites are essential for the desired product to be formed.

In summary, it is worth being noted that (a) a single oxide; either $Al_2O_3$ or MgO, does not significantly contribute to the conversion of benzoic acid and the yield of 2-ethylhexyl benzoate, but the acid-base pairs ($Mg^{2+}$–$O^{2-}$ and $Al^{3+}$–$O^{2-}$ pairs) do, (b) the conversion of benzoic acid appears to be governed by the ratio of acid/base density, (c) if possible, the catalysts, however, need to have both high acid density and the high base density for a high yield of 2-ethylhexyl benzoate, and (d) the compromise between the acid-base pair density and suitable acid-base strength would allow the high adsorption and conversion of reactants, and the high formation of the desired product.

### 3.4. Comparison with conventional catalysts

For comparison and benchmarking purposes, a conventional $Mg_3Al$-LDO was prepared using the similar co-precipitation method as applied to the AMO-$Mg_3AlO$ catalyst; but, instead of washing with the aqueous miscible organic solvent, the conventional LDO was washed with water. The conventional catalyst was then tested at the same reaction conditions. Subsequently, the physical properties and catalytic activity on synthesis of 2-ethylhexyl benzoate were compared with those of the AMO-$Mg_3AlO$ catalyst and some of previously reported catalysts. The results are shown in Tables 6 and 7, respectively. It is obvious that all chemical and physical properties of the AMO-$Mg_3AlO$ catalyst are significantly greater than those of the conventional one with the same Mg/Al ratio, owing to the AMO solvent treatment. Consequently, the AMO-

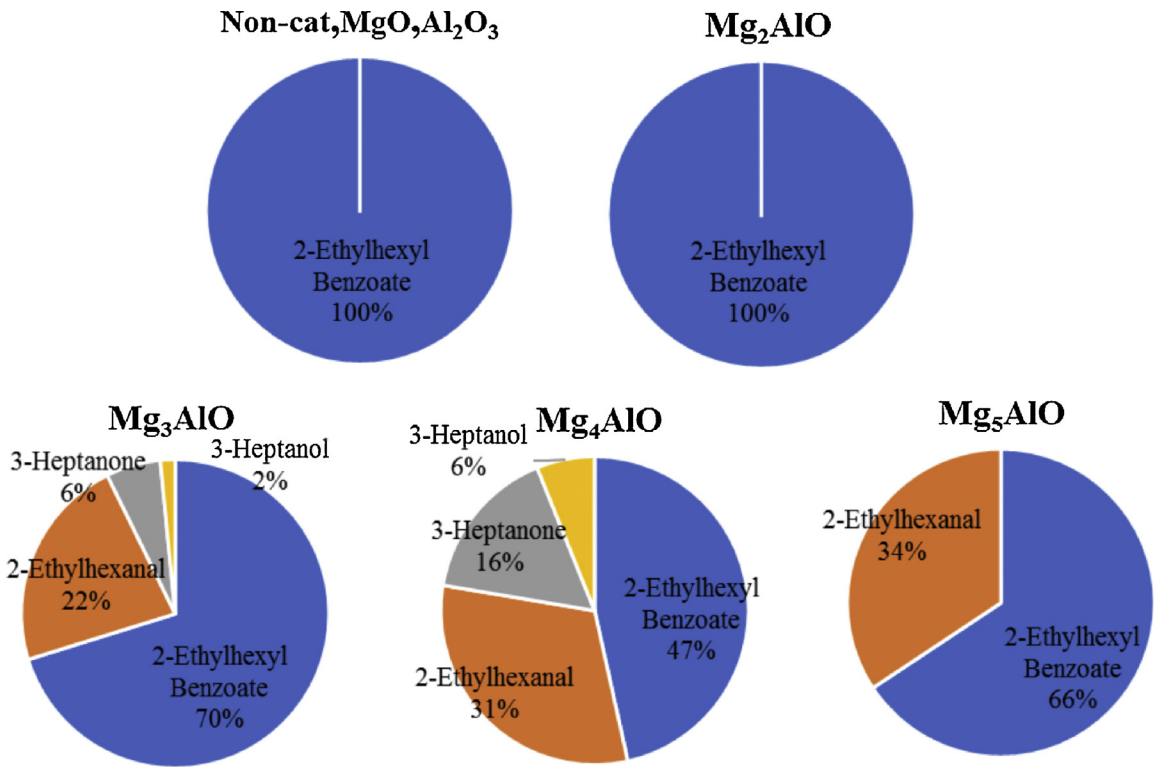


**Fig. 11.** Selectivity of products at time-on-stream of 10 h with and without a catalyst.

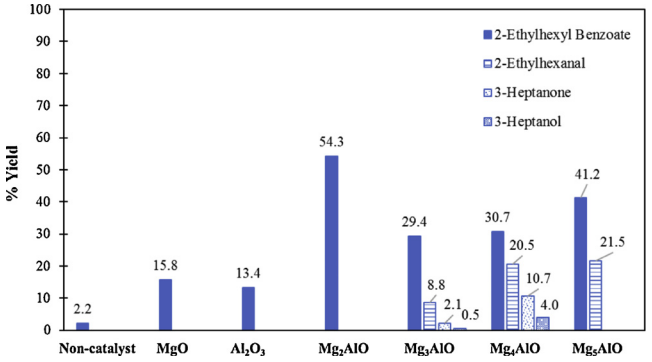


**Fig. 12.** Yield of products obtained from using the AMO-$Mg_xAlO$ catalysts.

$Mg_3AlO$ catalyst gives the tremendously-greater yield (three times higher) of 2-ethylhexyl benzoate than the conventional $Mg_3AlO$ one although it gives the slightly-higher conversion of benzoic acid. Moreover, it gives both higher conversion and yield than $Al_2O_3$ and MgO. Thus, it can be explained that the AMO-$Mg_3AlO$ catalyst has the significantly-higher density of acid-base pairs that can drives esterification pathway more selectively. Additionally, all AMO-$Mg_xAlO$ catalysts are benchmarked with some solid acid catalysts; namely, montmorillonite KSF, $Cs_{2.5}H_{0.5}PW_{12}O_{14}$ and sulfated $ZrO_2$ [1] (Table 7). Obviously, the AMO-$Mg_xAlO$ catalysts have superior performance than the other solid acid catalysts since they give a higher benzoic acid conversion and a greater yield of 2-ethylhexyl benzoate under lower temperature.

## 4. Conclusions

The AMO-$Mg_xAl$-$CO_3$ LDHs have been successfully synthesized in this work. After calcined at 500 °C, they were transformed to mixed oxide forms; however, the clay sheets were still preserved, as confirmed by the XRD, TGA, XPS, and XAS results. Moreover, they were found possessing both acidic and basic sites that vary with the Mg/Al ratio, which can change the acid-base properties of the materials. It has been proven that the density and strength of acidity and basicity was contributed from spinel ($MgAl_2O_4$), or the binary mixed oxide, according to the TPD and XAS results. Moreover, the coordination number observed from EXAFS analysis was found related with the acid-basic strength of the catalysts. The $Mg_xAlO$ mixed oxides derived from the AMO-layered double hydroxides were studied for their activity on the conversion of benzoic acid with 2-ethylhexanol. As a result, it was found that the conversion depended on acid-base pairs (both $Mg^{2+}-O^{2-}$ and $Al^{3+}-O^{2-}$ pairs) of the catalysts. The $Mg_5AlO$ and $Mg_4AlO$ catalysts can convert more than 63% benzoic acid to 2-ethylhexyl benzoate with around 30–41 % yield. The $Mg_2AlO$ catalyst gives the highest yield of 2-ethylhexyl benzoate. In conclusion, the selectivity of products depends on the phase compositions, elemental composition, and acid-base pairs sites ($Mg^{2+}-O^{2-}$ and $Al^{3+}-O^{2-}$ pairs).

**Table 6**
Chemical and physical properties of the conventional- and AMO-$Mg_3AlO$ catalysts in comparison.

| Catalyst | Surface Area ($m^2/g$)[a] | Pore Volume ($cm^3/g$)[a] | Pore Diameter (Å)[a] | Base density (mmol/g)[b] | Acid density (mmol/g)[c] |
|---|---|---|---|---|---|
| Conventional $Mg_3AlO$ | 186.8 | 0.7829 | 94.6 | 0.299 | 0.351 |
| AMO-$Mg_3AlO$ | 220.9 | 1.294 | 129 | 0.545 | 0.383 |

[a] Determined using BET.
[b] Determined using TPD-$CO_2$.
[c] Determined using TPD-$NH_3$.

**Table 7**
Catalytic performance of the conventional- and AMO-$Mg_3AlO$ catalysts in comparison with that of other previously-reported solid catalysts.

| Catalyst | Temp. (°C) | Reaction time | Conversion of benzoic acid (%) | Yield of 2-ethylhexyl benzoate (%) | Reference |
|---|---|---|---|---|---|
| AMO-$Mg_2AlO$ | 110 | 10 h | 54.3 | 54.3 | This work |
| AMO-$Mg_3AlO$ | | | 40.7 | 28.6 | |
| AMO-$Mg_4AlO$ | | | 66.1 | 30.7 | |
| AMO-$Mg_5AlO$ | | | 62.8 | 41.3 | |
| Conventional $Mg_3AlO$[a] | | | 39.6 | 9.2 | |
| MgO | | | 15.8 | 15.8 | |
| $Al_2O_3$ | | | 13.4 | 13.4 | |
| Montmorillonite KSF | 248 | 20.5 min | 34.7 | 4.7 | [1] |
| $Cs_{2.5}H_{0.5}PW_{12}O_{14}$ | 246 | 22 min | 17.3 | 3.3 | |
| Sulfated $ZrO_2$ | 251 | 22 min | 25.1 | 23.8 | |

[a] $Mg_3AlO$ catalyst was conventionally prepared using co-precipitation and then washed with water.

## Acknowledgements

This work was supported by SCG Chemicals, Co., Ltd., the Center of Excellence on Petrochemical and Materials Technology, and the Petroleum and Petrochemical College, Chulalongkorn University. The authors would like to acknowledge the great help and contribution from the 8th Beamline of the Siam Photon Laboratory, Synchrotron Light Research Institute (SLRI), Thailand.

## Appendix A. Supplementary data

Supplementary material related to this article can be found, in the online version, at doi:https://doi.org/10.1016/j.apcatb.2018.10.073.

## References

[1] G. Pipuš, I. Plazl, T. Koloini, Esterification of benzoic acid with 2-ethylhexanol in a microwave stirred-tank reactor, Ind. Eng. Chem. Res. 41 (2002) 1129–1134.
[2] M. Mekala, V.R. Goli, Kinetics of esterification of methanol and acetic acid with mineral homogeneous acid catalyst, Chin. J. Chem. Eng. 23 (2015) 100–105.
[3] A.L. Cardoso, S.C. Neves, M.J. da Silva, Kinetic study of alcoholysis of the fatty acids catalyzed by tin chloride (II): an alternative catalyst for biodiesel production, Energy Fuels 23 (2009) 1718–1722.
[4] T. Wenyu, Z. Zuoxiang, X. Weilan, L. Yingbin, T. Zhang, Kinetics of the mono-esterification between terephthalic acid and 1, 4-butanediol, Chin. J. Chem. Eng. 18 (2010) 391–396.
[5] J.-Y. Park, D.-K. Kim, J.-S. Lee, Esterification of free fatty acids using water-tolerable Amberlyst as a heterogeneous catalyst, Bioresour. Technol. 101 (2010) S62–S65.
[6] V.M. Mello, G.P. Pousa, M.S. Pereira, I.M. Dias, P.A. Suarez, Metal oxides as heterogeneous catalysts for esterification of fatty acids obtained from soybean oil, Fuel Process. Technol. 92 (2011) 53–57.
[7] S. Soltani, U. Rashid, R. Yunus, Y.H. Taufiq-Yap, Biodiesel production in the presence of sulfonated mesoporous ZnAl2O4 catalyst via esterification of palm fatty acid distillate (PFAD), Fuel 178 (2016) 253–262.
[8] K. Saravanan, B. Tyagi, H.C. Bajaj, Esterification of stearic acid with methanol over mesoporous ordered sulfated ZrO2–SiO2 mixed oxide aerogel catalyst, J. Porous Mater. 23 (2016) 937–946.
[9] A. Nagvenkar, S. Naik, J. Fernandes, Zinc oxide as a solid acid catalyst for esterification reaction, Catal. Commun. 65 (2015) 20–23.
[10] S. Nalli, D.G. Cooper, J.A. Nicell, Metabolites from the biodegradation of di-ester plasticizers by Rhodococcus rhodochrous, Sci. Total Environ. 366 (2006) 286–294.
[11] G. Tojo, M. Fernández, Oxidation of primary alcohols to carboxylic acids, A Guide to Current Common Practice, (2007).
[12] J. Di Cosimo, V. Dıez, M. Xu, E. Iglesia, C. Apesteguıa, Structure and surface and catalytic properties of Mg-Al basic oxides, J. Catal. 178 (1998) 499–510.
[13] L. Zhou, B. Dong, S. Tang, H. Ma, C. Chen, X. Yang, J. Xu, Sulfonated carbon catalyzed oxidation of aldehydes to carboxylic acids by hydrogen peroxide, J. Energy Chem. 22 (2013) 659–664.
[14] V. Walker, G.A. Mills, Urine 4-heptanone: a β-oxidation product of 2-ethylhexanoic acid from plasticisers, Clin. Chim. Acta 306 (2001) 51–61.
[15] K. Parida, J. Das, Mg/Al hydrotalcites: preparation, characterisation and ketonisation of acetic acid, J. Mol. Catal. A Chem. 151 (2000) 185–192.
[16] A. Dahlén, G. Hilmersson, Chelating alcohols accelerate the samarium diiodide mediated reduction of 3-heptanone, Tetrahedron Lett. 42 (2001) 5565–5569.
[17] T. Ikariya, A.J. Blacker, Asymmetric transfer hydrogenation of ketones with bifunctional transition metal-based molecular catalysts, Acc. Chem. Res. 40 (2007) 1300–1308.
[18] R. Noyori, T. Ohkuma, Asymmetric catalysis by architectural and functional molecular engineering: practical chemo-and stereoselective hydrogenation of ketones, Angew. Chemie Int. Ed. 40 (2001) 40–73.
[19] V. Erastova, M.T. Degiacomi, D. OHare, C. Greenwell, Understanding surface interactions in aqueous miscible organic solvent treated layered double hydroxides, RSC Adv. 7 (2017) 5076–5083.
[20] C. Chen, M. Yang, Q. Wang, J.-C. Buffet, D. O'Hare, Synthesis and characterisation of aqueous miscible organic-layered double hydroxides, J. Mater. Chem. A 2 (2014) 15102–15110.
[21] V. Diez, C. Apesteguia, J. Di Cosimo, Effect of the chemical composition on the catalytic performance of Mg yAlO x catalysts for alcohol elimination reactions, J. Catal. 215 (2003) 220–233.
[22] O.D. Pavel, D. Tichit, I.-C. Marcu, Acido-basic and catalytic properties of transition-metal containing Mg–Al hydrotalcites and their corresponding mixed oxides, Appl. Clay Sci. 61 (2012) 52–58.
[23] T. Kawabata, T. Mizugaki, K. Ebitani, K. Kaneda, Highly efficient esterification of carboxylic acids with alcohols by montmorillonite-enwrapped titanium as a heterogeneous acid catalyst, Tetrahedron Lett. 44 (2003) 9205–9208.
[24] X. Li, J. Zhu, Q. Liu, B. Wu, The removal of naphthenic acids from dewaxed VGO via esterification catalyzed by Mg–Al hydrotalcite, Fuel Process. Technol. 111 (2013) 68–77.
[25] Y. Jia, Y. Fang, Y. Zhang, H.N. Miras, Y.F. Song, Classical keggin intercalated into layered double hydroxides: facile preparation and catalytic efficiency in knoevenagel condensation reactions, Chem. Eur. J. 21 (2015) 14862–14870.
[26] S. Shylesh, D. Kim, A.A. Gokhale, C.G. Canlas, J.O. Struppe, C.R. Ho, D. Jadhav, A. Yeh, A.T. Bell, Effects of composition and structure of Mg/Al oxides on their activity and selectivity for the condensation of methyl ketones, Ind. Eng. Chem. Res. 55 (2016) 10635–10644.
[27] M. Hájek, P. Kutálek, L. Smoláková, I. Troppová, L. Čapek, D. Kubička, J. Kocík, D.N. Thanh, Transesterification of rapeseed oil by Mg–Al mixed oxides with various Mg/Al molar ratio, Chem. Eng. J. 263 (2015) 160–167.
[28] D. Wan, H. Liu, R. Liu, J. Qu, S. Li, J. Zhang, Adsorption of nitrate and nitrite from aqueous solution onto calcined (Mg–Al) hydrotalcite of different Mg/Al ratio, Chem. Eng. J. 195 (2012) 241–247.
[29] J.A. van Bokhoven, J.C. Roelofs, K.P. de Jong, D.C. Koningsberger, unique structural properties of the Mg–Al hydrotalcite solid base catalyst: an in situ study using Mg and Al K-edge xafs during calcination and rehydration, Chem. Eur. J. 7 (2001) 1258–1265.
[30] J.-H. Choy, Y.-M. Kwon, K.-S. Han, S.-W. Song, S.H. Chang, Intra-and inter-layer structures of layered hydroxy double salts, Ni 1 − x Zn 2x (OH) 2 (CH 3 CO 2) 2x· nH 2 O, Mater. Lett. 34 (1998) 356–363.
[31] H.K.D. Nguyen, T.D. Nguyen, D.N. Hoang, D.S. Dao, T.T. Nguyen, L. Wanwisa, L.L. Hoang, X-ray absorption spectroscopies of Mg-Al-Ni hydrotalcite like compound for explaining the generation of surface acid sites, Korean J. Chem. Eng. (2015) 1–6.
[32] M. Del Arco, P. Malet, R. Trujillano, V. Rives, Synthesis and characterization of hydrotalcites containing Ni (II) and Fe (III) and their calcination products, Chem. Mater. 11 (1999) 624–633.
[33] Z.P. Xu, J. Zhang, M.O. Adebajo, H. Zhang, C. Zhou, Catalytic applications of layered double hydroxides and derivatives, Appl. Clay Sci. 53 (2011) 139–150.
[34] J. Haber, Manual on catalyst characterization (recommendations 1991), Pure Appl. Chem. 63 (1991) 1227–1246.
[35] M.M. Rao, B.R. Reddy, M. Jayalakshmi, V.S. Jaya, B. Sridhar, Hydrothermal synthesis of Mg–Al hydrotalcites by urea hydrolysis, Mater. Res. Bull. 40 (2005) 347–359.
[36] J.R. Lindsay, H.J. Rose, W.E. Swartz, P.H. Watts, K.A. Rayburn, X-ray photoelectron spectra of aluminum oxides: structural effects on the "chemical shift", Appl. Spectrosc. 27 (1973) 1–5.
[37] L.-X. Li, D. Xu, X.-Q. Li, W.-C. Liu, Y. Jia, Excellent fluoride removal properties of porous hollow MgO microspheres, New J. Chem. 38 (2014) 5445–5452.
[38] G. Hincapié, D. López, A. Moreno, Infrared analysis of methanol adsorption on mixed oxides derived from Mg/Al hydrotalcite catalysts for transesterification reactions, Catal. Today 302 (2018) 277–285.
[39] J. Shen, M. Tu, C. Hu, Structural and surface acid/base properties of hydrotalcite-derived MgAlO oxides calcined at varying temperatures, J. Solid State Chem. 137 (1998) 295–301.
[40] P. Kuśtrowski, D. Sułkowska, L. Chmielarz, A. Rafalska-Łasocha, B. Dudek,

R. Dziembaj, Influence of thermal treatment conditions on the activity of hydrotalcite-derived Mg–Al oxides in the aldol condensation of acetone, Microporous Mesoporous Mater. 78 (2005) 11–22.
[41] I.-C. Marcu, N. Tanchoux, F. Fajula, D. Tichit, Catalytic conversion of ethanol into butanol over M–Mg–Al mixed oxide catalysts (M= Pd, Ag, Mn, Fe, Cu, Sm, Yb) obtained from LDH precursors, Catal. Letters 143 (2013) 23–30.
[42] S. Cadars, G. Layrac, C. Gérardin, M. Deschamps, J.R. Yates, D. Tichit, D. Massiot, Identification and quantification of defects in the cation ordering in Mg/Al layered double hydroxides, Chem. Mater. 23 (2011) 2821–2831.
[43] H. Wang, W. Duan, Y. Lei, Y. Wu, K. Guo, X. Wang, An intracrystalline catalytic esterification reaction between ethylene glycol intercalated layered double hydroxide and cyclohexanecarboxylic acid, Catal. Commun. 62 (2015) 44–47.